

Advances and challenges in impedance-based structural health monitoring

Thanh-Canh Huynh^a, Ngoc-Loi Dang^b and Jeong-Tae Kim^{*}

*Department of Ocean Engineering, Pukyong National University,
599-1 Daeyon-3dong, Nam-gu, Busan 608-737, Republic of Korea*

(Received November 15, 2017, Revised December 2, 2017, Accepted December 4, 2017)

Abstract. Impedance-based damage detection method has been known as an innovative tool with various successful implementations for structural health monitoring of civil structures. To monitor the local critical area of a structure, the impedance-based method utilizes the high-frequency impedance responses sensed by piezoelectric sensors as the local dynamic features. In this paper, current advances and future challenges of the impedance-based structural health monitoring are presented. Firstly, theoretical background of the impedance-based method is outlined. Next, an overview is given to recent advances in the wireless impedance sensor nodes, the interfacial impedance sensing devices, and the temperature-effect compensation algorithms. Various research works on these topics are reviewed to share up-to-date information on research activities and implementations of the impedance-based technique. Finally, future research challenges of the technique are discussed including the applicability of wireless sensing technology, the predetermination of effective frequency bands, the sensing region of impedance responses, the robust compensation of noise and temperature effects, the quantification of damage severity, and long-term durability of sensors.

Keywords: impedance responses; wireless impedance sensor; PZT interface; temperature effect; damage detection; structural health monitoring

1. Introduction

The process of implementing a damage detection and characterization strategy for engineering structures is referred to structural health monitoring (SHM) (Balageas *et al.* 2006). Depending upon the inspected regions of the target structure, the SHM could be classified into global SHM, local SHM and hybrid SHM. The global SHM usually deals with using low-frequency dynamic features (e.g., modal parameters) or structural deformation (e.g., deflection or inclination) to characterize the integrity of a whole structure. In a typical way, the global SHM employs acceleration responses obtained from several distributed sensors on the structure to monitor the changes in structural characteristics caused by damage. However, this method utilizes low-frequency vibration responses that are not very sensitive to localized small-size damage. On the

*Corresponding author, Professor, E-mail: idis@pknu.ac.kr

^aPost-doctoral Researcher, E-mail: ce.huynh@gmail.com

^bDoctoral Student, E-mail: loi.ngocdang@gmail.com

other hand, the local SHM utilizes high-frequency features (such as electromechanical impedance, acoustics, ultrasonic guided waves, and infrared microwaves) to assess the integrity of local regions close to the sensor. By employing the high-frequency responses, the local SHM techniques have been very effective to assess the structural condition of local critical members in civil structures. The hybrid SHM refers to a combination of local and global responses to achieve more efficient SHM systems for complex civil structures (Kim *et al.* 2010, Hou *et al.* 2014). By employing multi-metric data, the hybrid SHM systems could provide better damage monitoring results than single-metric information (Studer and Peters 2004, Ho *et al.* 2012).

Lessons accumulated from the recent tragic disasters indicate that the failure of critical structural connections in civil structures carries the potentials that could lead to the catastrophic collapse of whole structures (Lee 1996, National Transportation Safety Board 2008, Burgoyne and Scantlebury 2008). In civil structures, critical structural connections are referred as local members where the 'hot spots' of the concerned structure are expected. These local critical connections are often guessed by the calculation or experience with other similar structures. Among various local SHM techniques, the electromechanical (EM) impedance-based SHM has been found as an innovative and powerful approach to detect the local damage for various types of structures. To detect structural changes induced by damage at critical areas, the impedance-based method utilizes the EM impedance sensed by piezoceramic patches such as PZT (i.e., lead zirconate titanate) as the local dynamic features (Liang *et al.* 1994). Since the EM impedance response contains the information about the structural status, any damage occurred in the structural systems can be diagnosed by quantifying the variation of the measured impedance signals.

The impedance-based method utilizes the high-frequency excitation that is commonly in ultrasonic frequency bands. The short wavelengths associated with the high frequencies allow this technique to sensitively capture the incipient damage occurred in the critical member of civil structures. Stokes and Clouds (1993) discussed the wavelength of excitation should be smaller than the characteristic length of the damage to be detected. Also, Sun *et al.* (1995) suggested a guideline for the selection of frequency ranges to monitor damage by using impedance responses. Esteban (1996) investigated the sensing region of the impedance-based method by extensive numerical modeling based on the wave propagation theory. The primary advantages of the impedance-based approach can be summarized as (1) the technique is not model-based, and thus can be easily applied to complex structures; (2) the technique uses small, cheap, lightweight, fast response, and non-intrusive sensors to monitor inaccessible locations; (3) the technique itself, using high-frequency responses, is very sensitive to minor structural damage; (4) the measured data can be easily interpreted; and (5) the technique can be integrated with the wireless sensing technology to achieve a smart SHM system.

So far, the impedance-based technique has been applied for health monitoring of truss structures (Sun *et al.* 1995), reinforced concrete structures (Soh *et al.* 2000, Hu *et al.* 2014), steel joints (Ayres *et al.* 1998, Park *et al.* 2003, Ho *et al.* 2014, Huynh and Kim 2014, Huynh *et al.* 2015a and 2015b, Ryu *et al.* 2017), steel pipeline systems (Park *et al.* 2003), thin plates and aerospace structures (Giurgiutiu and Zagari 2005, Lim *et al.* 2011, Bilgunde and Bond 2017, Zahedi and Huang 2017), rocks (Yang *et al.* 2008), timber specimens (Wang *et al.* 2016), and wind turbine structures (Nguyen *et al.* 2017). Despite the successful evaluations of the technique for structural health monitoring of civil structures, there exist practical issues that have caused inevitable uncertainties in impedance measurements as well as feature extractions. This is because real structures exist in an environment of ambient induced noises, vibrations, external loads, temperature effects, and so on. These effects should be dealt appropriately in practical applications

of the impedance-based technique (Lim *et al.* 2011, Lim and Soh 2012, Park *et al.* 2015, Yang *et al.* 2015, Huynh *et al.* 2016a, Huynh and Kim 2017a).

In this paper, current advances and future challenges of the impedance-based structural health monitoring are presented. Firstly, theoretical background of the impedance-based method is outlined. Next, an overview is given to recent advances in the wireless impedance sensor nodes, the interfacial impedance sensing devices, and the temperature-effect compensation algorithms. Various research works on these topics are reviewed to share up-to-date information on research activities and implementations of the impedance-based technique. Finally, future research challenges of the technique are discussed including the applicability of wireless sensing technology, the predetermination of effective frequency bands, the sensing region of impedance responses, the robust compensation of noise and temperature effects, the quantification of damage severity, and long-term durability of sensors.

2. Theoretical background

2.1 Piezoelectric sensors

Piezoelectric materials are the ones that possess the piezoelectric properties of converting mechanical energy into electrical energy and vice versa. A mechanical strain applied to a piezoelectric material generates charges on the surface (i.e., ‘direct piezoelectric effect’). Vice versa, the piezoelectric material is deformed when an electrical voltage is applied (i.e., ‘inverse piezoelectric effect’). Many materials, both natural and synthetic, exhibit piezoelectric properties such as quartz (SiO_2), berlinite (AlPO_4), gallium orthophosphate (GaPO_4), tourmaline, barium titanate (BaTiO_3), lead zirconate titanate (PZT), zinc oxide (ZnO), aluminum nitride (AlN), and polyvinylidene fluoride (PVDF). Some of them are shown in Fig. 1. Such materials are considerably important in SHM that offers the great opportunity for creating smart, effective and efficient SHM systems. Among those piezoelectric materials, PZT is considered today one of the most economical piezoelectric elements with a huge market of products. PZT patches are small and unobtrusive. The cost is less than \$10 for each, but they are applicable to high-frequency applications at hundreds of kHz and beyond (Giurgiutiu 2014).

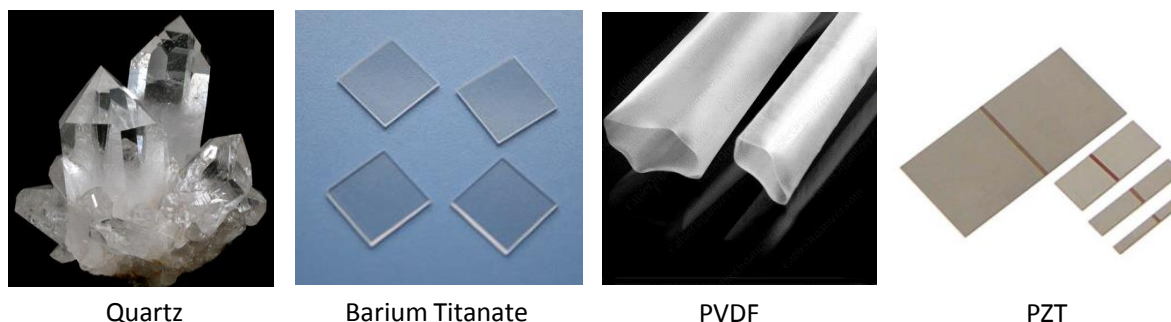


Fig. 1 Natural and synthetic piezoelectric materials

The piezoelectric principles can be characterized by the electromechanical constitutive equations in a strain-charge relation can be expressed by tensor form as follows (Giurgiutiu 2014):

$$\text{Direct piezoelectric effect: } D_i = \varepsilon_{ij}^T E_j + d_{im} T_m \quad (1)$$

$$\text{Inverse piezoelectric effect: } S_k = d_{jk} E_j + s_{km}^E T_m \quad (2)$$

where D_i is the electrical displacement; ε_{ij}^T is the dielectric permittivity constant; E_j is the applied electric field; and d_{im} and d_{jk} are the piezoelectric coefficients; T_m is the stress vector; S_k is the strain vector; and s_{km}^E is the elastic compliance of the piezoelectric material at a zero electric field. The superscript T and E denote that the quantity is measured at constant stress and constant electric field, respectively. The subscripts denote the direction of the electric field and the associated mechanical strain, respectively. Eqs. (1) and (2) establish relationships between the electrical and elastic properties of a piezoelectric material.

Due to the dual piezoelectric effects, a piezoelectric material can be used for sensing structural deformation via the direct piezoelectric effect and actuating the structure via the inverse effect. Figure 2 illustrates a single-layer piezoelectric material used for sensing and actuating according to the direction of deformation (d_{3x} effect). The piezoelectric material can be generalized for two modes which are particularly important when defining the electromechanical coupling coefficient (Sodano *et al.* 2004). The first operates in the longitudinal mode (d_{33} effect see Fig. 2(a)) and the second operates in the transverse mode (d_{31} effect see Fig. 2(b)). As a piezoelectric actuator, in the longitudinal mode (d_{33} effect), the electric field is applied in the '3' direction and the material is strained in the polling or '3' direction. In the transverse mode (d_{31} effect), the electric field is applied in the '3' direction and the material is strained in the '1' direction or perpendicular to the poling direction. As a piezoelectric sensor, when the strain field is applied to the material in the '3' direction (the longitudinal mode) or the '1' direction (the transverse mode), the electric field is generated that tried to return the material to its original shape.

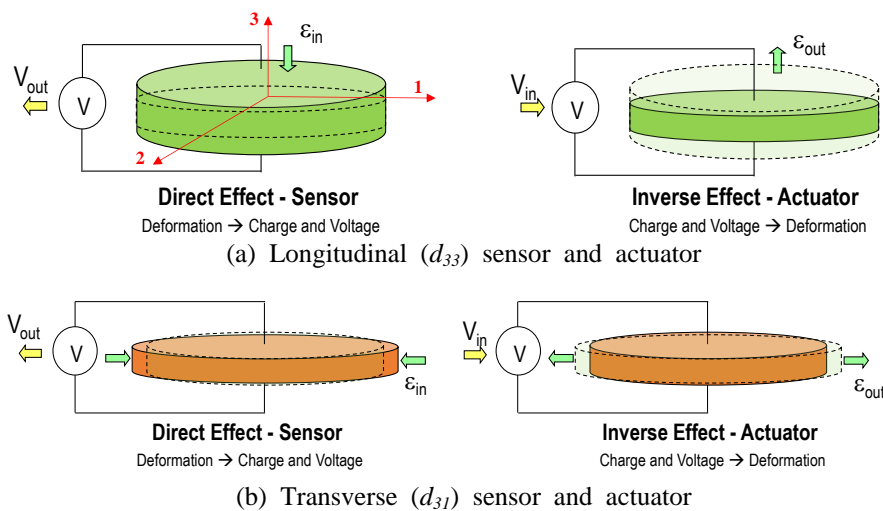


Fig. 2 Single-layer piezoelectric sensors and actuators (Piezo Systems 2016)

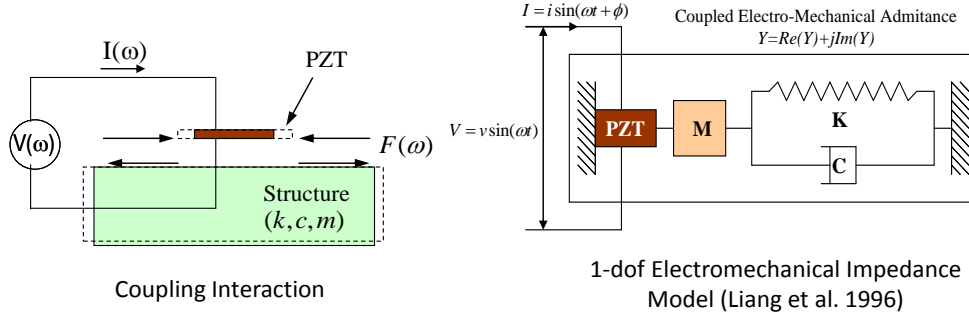


Fig. 3 Electromechanical interaction between PZT and host structure

2.2 Impedance-based damage detection

By using a piezoelectric material as an actuator, Liang *et al.* (1994) theoretically proposed the concept of the EM impedance for a piezoelectric actuator-driven mechanical system, which is based on the coupling of mechanical and electrical characteristics. Liang's pioneering studies have laid the groundwork for SHM of civil structures using the EM impedance.

As shown in Fig. 3, a piezoelectric patch (e.g., PZT) is surface-bonded to the structure at examined region. The interaction between the PZT and the structure can be simply explained by 1-DOF free-body diagram of a PZT-structure system (Liang *et al.* 1996). Due to inverse piezoelectric effect, an input harmonic voltage $V(\omega)$ induces a deformation of PZT. At the same time, a force $F(\omega)$ against that deformation is induced into the structure and the PZT. The coupling between the electrical impedance of the PZT sensor $Z_a(\omega)$ and the structural mechanical (SM) impedance of the host structure $Z_s(\omega)$ can be simplified as follows (Liang *et al.* 1996):

$$Z(\omega) = \frac{V}{I} = \left\{ i\omega \frac{w_a l_a}{t_a} \left[\hat{\epsilon}_{33}^T - \frac{1}{Z_a(\omega)/Z_s(\omega) + 1} d_{31}^2 \hat{Y}_{11}^E \right] \right\}^{-1} \quad (3)$$

where $\hat{Y}_{11}^E = (1 + i\eta)Y_{11}^E$ is the complex Young's modulus of the PZT patch at a zero electric field; $\hat{\epsilon}_{33}^T = (1 - i\delta)\epsilon_{33}^T$ is the complex dielectric constant at zero stress; d_{31} is the piezoelectric coupling constant in l -direction at zero stress; and w_a , l_a , and t_a are the width, length, and thickness of the piezoelectric patch, respectively. The parameters η and δ are structural damping loss factor and dielectric loss factor of piezoelectric material, respectively.

For the 1-DOF system shown in Fig. 3, the SM impedance of the host structure $Z_s(\omega)$ is obtained by the ratio of force $F(\omega)$ to velocity $\dot{u}(\omega)$, as follows:

$$Z_s(\omega) = \frac{F(\omega)}{\dot{u}(\omega)} = c + m \frac{\omega^2 - \omega_n^2}{\omega} i \quad (4)$$

where c and m are the damping coefficient and the mass of the structure, respectively; ω_n is the angular natural frequency of the structure; and ω is the angular frequency of the excitation voltage.

From Eqs. (3) and (4), it is obvious that the EM impedance is a function of dynamic parameters of the host structure. Therefore, the change in these parameters induced by damage can be represented by the change in the EM impedance. In damage monitoring, the sensitivity of the impedance-based method is closely related to the frequency band selected. The frequency band of impedance signatures should be selected appropriately in order to realize the structural changes in the host structure. The frequency band that is sensitive to the structural damage is known as the 'effective frequency band'.

Generally, if the excitation frequency is not identical to the natural frequency of the structure (i.e., $\omega \neq \omega_n$), the SM impedance takes the full term of Eq. (4). In this case, the SM impedance of the structure is very significant compared with the mechanical impedance of the PZT (i.e., $Z_s(\omega) \gg Z_a(\omega)$). As the result, the term $Z_a(\omega)/Z_s(\omega)$ is neglected and the EM impedance is approximated as (Nguyen and Kim 2012):

$$Z(\omega) \approx \left\{ i\omega \frac{w_a l_a}{t_a} \left[\varepsilon_{33}^T - d_{31}^2 \hat{Y}_{11}^E \right] \right\}^{-1} \quad (5)$$

In Eq. (5), the contribution of the SM impedance to the EM impedance is filtered out. Therefore, the structural change may not be identified sensitively by the EM impedance.

On the other hand, if the PZT sensor is excited by a frequency matching with the natural frequency of the structure (i.e., $\omega = \omega_n$), the SM impedance takes only the term of the damping coefficient (i.e., $Z_s(\omega) = c$). Thus, the SM impedance for that frequency is comparable with the mechanical impedance of the PZT, and the EM impedance is expressed as

$$Z(\omega) = \left\{ i\omega \frac{w_a l_a}{t_a} \left[\varepsilon_{33}^T - \frac{1}{Z_a / c + 1} d_{31}^2 \hat{Y}_{11}^E \right] \right\}^{-1} \quad (6)$$

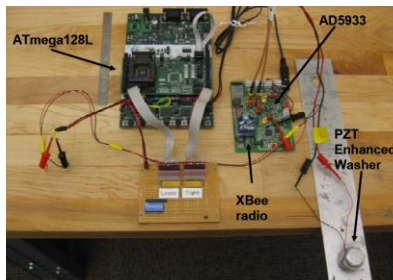
In Eq. (6), the contribution of the SM impedance to the EM impedance is the damping coefficient c . This contribution is reflected by the resonant peak in the impedance signatures at the correspondent frequency. In other words, the EM impedance at resonance represents not only the modal damping but also the natural frequency of the structure. Therefore, the structural changes due to the damage event could be identified sensitively by the change in the EM impedance at the resonant frequency range (i.e., effective frequency range). For a given target structure, the effective frequency range is unknown and should be predetermined before real impedance-based implementations.

Since the EM impedance response contains the information about the structural status, any damage occurred in the structural systems can be diagnosed by quantifying the variation of the measured impedance signals. To quantify the impedance changes, statistical damage indices have been widely used. Sun *et al.* (1995) proposed a simple statistical algorithm based on the root mean square deviation (i.e., RMSD) of impedance signatures. Raju (1998) suggested another method based on the correlation coefficient (i.e., CC) of impedance signatures. Zagrai and Giurgiutiu (2001) investigated several statistical damage classification methods including the RMSD, mean absolute percentage deviation, covariance change, and correlation coefficient deviation (i.e., CCD).

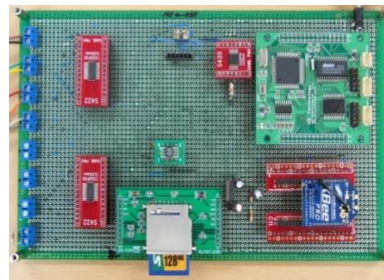
3. Wireless impedance sensor technology

3.1 Recent wireless impedance sensor nodes

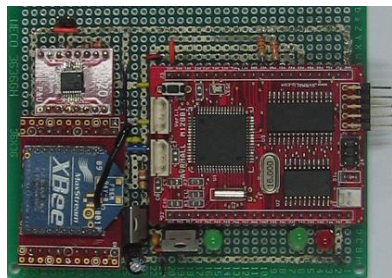
Conventionally, the EM impedance is measured using impedance analyzers like HIOKI 3532 or HP4194A which are high-performance, bulky size, and high-cost devices. Such impedance analyzers are inconvenient to be implemented out of the laboratory and may not be attractive for online impedance-based SHM. In addition, today’s civil structures are very complex and they often consist of numerous critical members. To establish a SHM system for such target structures, a large number of sensing channels are required. In the recent years, the development of wireless sensor networks has opened a new paradigm with automated, cost-efficient monitoring systems for SHM (Lynch *et al.* 2003, Spencer *et al.* 2004, Nagayama 2007, Kim *et al.* 2011, Ho *et al.* 2012, and Kim *et al.* 2013 and 2014, Huynh *et al.* 2016b).



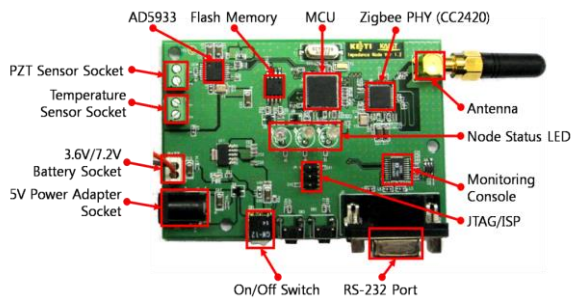
Mascarenas *et al.* (2007)



Park S. *et al.* (2009)



Park J. (2009)



Min *et al.* (2010)



Perera *et al.* (2017)

Fig. 4 Recent developments of wireless impedance sensing devices

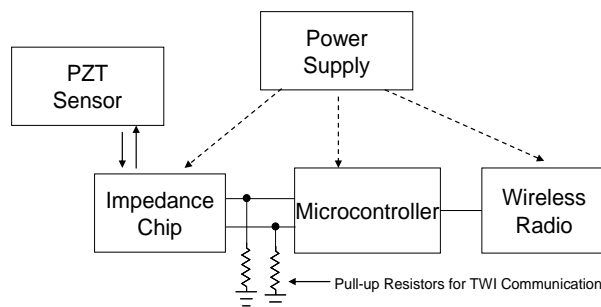


Fig. 5 Schematic of wireless impedance sensor node by Park (2009)

Research efforts have been made to integrate MEMS (i.e., micro-electromechanical systems) and radio-frequency telemetry-based sensing schemes with the impedance-based SHM method to achieve a smart SHM system with less resources and more reliability (Mascarenas *et al.* 2007, Park *et al.* 2009, Park *et al.* 2010, Min *et al.* 2010, and Kim *et al.* 2011, and Nguyen *et al.* 2011, Perera *et al.* 2017). Figure 4 illustrates wireless impedance sensing devices developed in the recent years. The first prototype of wireless impedance sensor node was proposed by Mascarenas *et al.* (2007). Since then, many researchers have improved the initial prototype to achieve a low-cost multifunctional wireless impedance sensor node. Park *et al.* (2009) embedded more functions into the first prototype such as temperature recording, multi-channel measurement, and SD memory card slot. Min *et al.* (2010) embedded damage detection/sensor self-diagnosis algorithms as well as power management with energy harvesters. Perera *et al.* (2017) proposed a flexible wireless impedance sensor framework, with the aim to provide the stable software and reliable hardware suitable for full-scale and autonomous SHM. Up-to-date, the wireless impedance sensors are designed based on the low-cost impedance chip AD5933 (Analog Devices 2010).

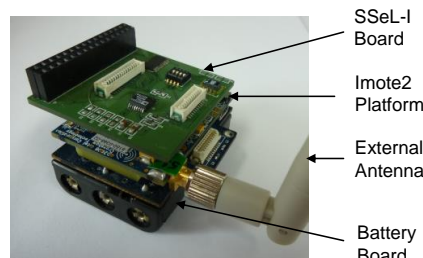
3.2 Wireless impedance sensor node by PKNU

The research group at the Pukyong National University (PKNU) has developed smart wireless impedance sensor nodes (Park 2009, and Kim *et al.* 2011, Nguyen *et al.* 2011). Park (2009) proposed a low-cost wireless sensor node with only \$100, the so-called 'Imp-SSN' (see Fig. 4). The Imp-SSN consists of the power supply, PZT sensor, impedance chip, microcontroller, and wireless radio, as shown in Fig. 5. The Imp-SSN integrates a low-cost impedance chip AD5933 (Analog Devices 2010) for measuring and recording the EM impedance. The AD5933 impedance chip has the following embedded multi-functional circuits: function generator, digital-to-analog converter, current-to-voltage amplifier, anti-aliasing filter, ADC, and discrete Fourier transform (DFT) analyzer. A microcontroller ATmega128L is used for controlling and computing, and a radio-frequency module XBee (2.4 GHz Zigbee) for wirelessly transmitting the data. The microcontroller ATmega128L has 8 bits of bus size, 0-16 MHz clock speed, 32 kB RAM and a 128 kB flash memory.

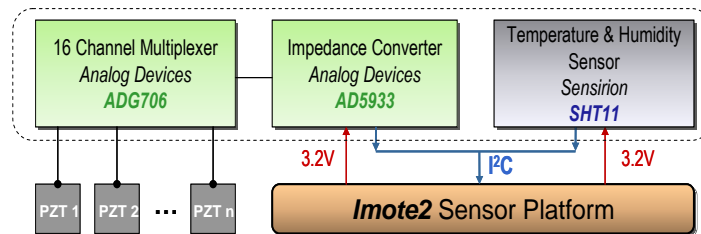
By adopting the same low-cost impedance chip (i.e., AD5933), Kim *et al.* (2011) have developed an impedance sensor board SSeL-I that was integrated with Imote2 sensor platform (Nagayama *et al.* 2009) for the high-speed measurement. Nguyen *et al.* (2011) have modified the combined Imote2/SSeL-I sensor node to wirelessly measure EM impedances from multiple PZT patches. The design schematic of the Imote2/SSeL-I is given in Fig. 6. As shown in Fig. 6(a), the

sensor node has three layers: a battery board, the Imote2 sensor platform, and the SSeL-I sensor board. The Imote2 platform is designed with a PXA27x processor (Memsic Co. 2010) which has a clock speed of 13-416 MHz, SRAM of 256 kB, flash memory of 32 MB and SDRAM of 32 MB. This platform also integrates with many I/O options and a wireless radio CC2420 (2.4 GHz Zigbee RF) for data transmission. The large memory and high operating speed of Imote2 allow it enable advanced and complicated SHM techniques.

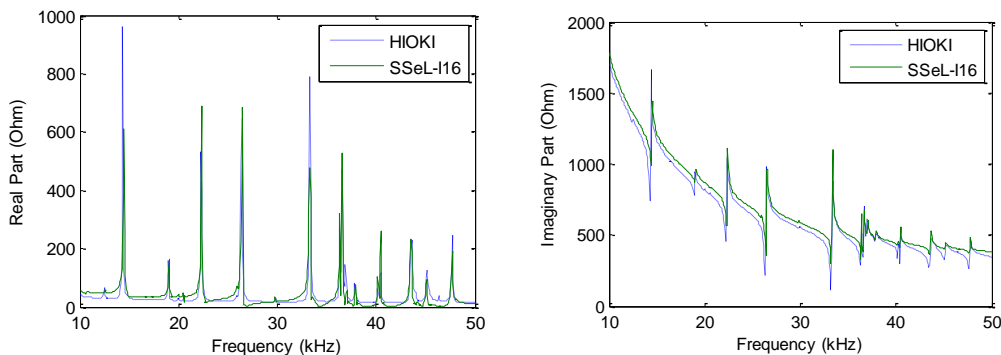
As shown in Fig. 6(b), the Imote2 platform is utilized for controlling impedance measurement, and for wireless communication by the on-board microcontroller PXA27x and wireless radio CC2420. Note that the wireless transmitting distance can be expanded up to 125 m by using an external antenna connected to the Imote2 platform. The AD5933 impedance chip of the sensor node has the capability to measure electric impedance up to 100 kHz. The AD5933 interacts with an ADG706 multiplexer to allow monitoring EM impedance from up to sixteen PZT sensors by a single sensor node. An SHT11 sensor is also integrated into SSeL-I board to monitor temperature and humidity of the environment (see Nguyen *et al.* 2011 for details on the operation of the Imote2/SSeL-I sensor node).



(a) SSeL-I prototype



(b) Schematic of SSeL-I



(c) Impedance signatures of a PZT-aluminum plate measured by wired and wireless systems

Fig. 6 SSeL-I wireless impedance sensor node (Nguyen *et al.* 2011)

As shown in Fig. 6(c), the wireless SSeL-I impedance sensor showed consistent impedance signatures with the wired HIOKI-3532 for the impedance measurement of a PZT-aluminum structure.

The applicability of the SSeL-I impedance sensor node was also evaluated on long-term impedance monitoring for the Hwamyung cable-stayed bridge located in Busan (Korea), as shown in Fig. 7. Total six smart impedance sensor nodes including one gateway node were installed on the bridge for impedance measurements of the cable system, see Fig. 7(a). The impedance signatures were measured in the frequency range of 10-100 kHz with 500 intervals of sweeping frequency. The variation of the impedance responses of the anchorages according to the variation of ambient temperature was observed, see Fig. 7(b). It is observed that when the temperature slightly went up from 26°C to 30°C, the real impedance signatures shifted to right side indicating the increment in the anchorage's impedance frequency.

The specification of the Imote2/SSeL-I sensor node is compared to one of the commercial impedance analyzers HIOKI3532, as listed in Table 1. Despite a narrow frequency range (1 kHz – 100 kHz), the Imote2/SSeL-I sensor node is much more economical than the conventional wired HIOKI3532 impedance analyzer.

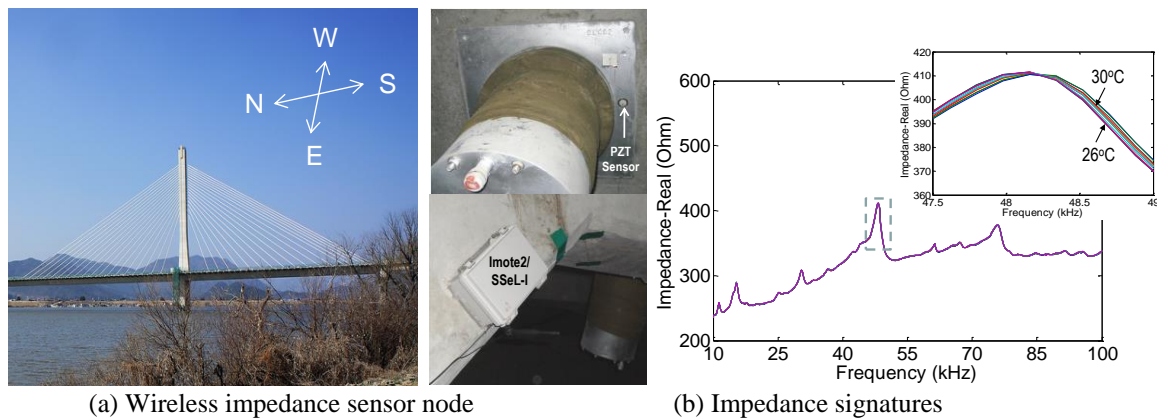


Fig. 7 Wireless impedance measurements of Hwamyung cable-stayed bridge (Ho *et al.* 2012)

Table 1 Wireless Imote2/SSeL-I versus wired HIOKI impedance analyzer

Feature	Imote2/SSeL-I	Commercial HIOKI
Model	AD5933	HIOKI3532
Impedance range	1 k Ω - 10 k Ω	10 k Ω - 200 k Ω
Frequency range	1 kHz - 100 kHz	42 Hz - 5 MHz
Excitation voltage	1.98 V _{p-p}	14 V _{p-p}
Dimensions	45×45×12 mm	352×323×124 mm
Weight	12 g	6.5 kg
Cost	\$US 300	\$US 15,000

4. PZT Interface-based impedance monitoring technique

4.1 PZT interface technique

As stated previously, the determination of effective frequency bands in impedance monitoring practices is a target-dependent problem. For most cases, the effective frequency range of a given structure is unknown and traditionally identified by try-and-errors or experiences on similar structures. So far, the wireless impedance sensing technology has relied on the low-cost impedance chip AD5933 that allows a measurable frequency range only within 1-100 kHz (Min *et al.* 2010 and Kim *et al.* 2011). However, many target structures require the EM impedance signal to be measured in higher frequency ranges (i.e., over 100 kHz) to sensitively capture incipient damage (Chaudhry *et al.* 1995, Soh *et al.* 2000, Park *et al.* 2003, Kim *et al.* 2010, and Annamdas 2012). For example, Kim *et al.* (2010) conducted the impedance monitoring in the prestressed tendon-anchorage of a PSC girder. Their study found that the effective frequency band was very significant, even above 800 kHz (see Fig. 8). To enable wireless impedance sensing in such target structures, the effective frequency band is needed to be reduced to below 100 kHz.

The PZT interface technique can be a solution to predetermine effective frequency bands of impedance responses and to reduce them to below 100 kHz for the wireless impedance sensing. The PZT interface device is an interfacial structure equipped with a PZT sensor, as shown in Fig. 9. Park (2009) developed the so-called ‘PZT interface washer’ tailored to the impedance monitoring of the prestressed joints, as shown in Fig. 9(a). This type is needed to be pre-installed during the construction of joints; therefore, it is impossible to apply it into existing connections.

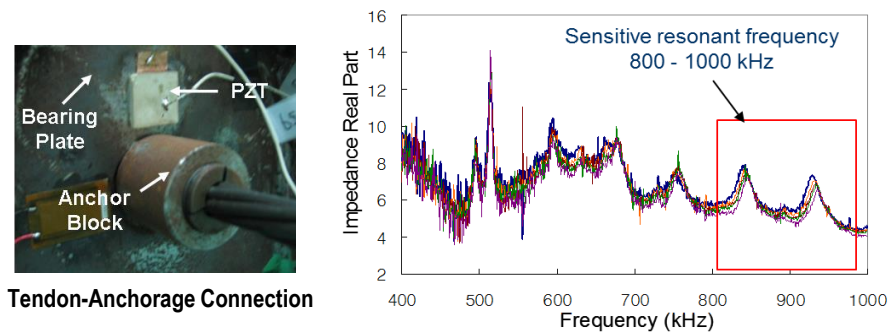


Fig. 8 Sensitive frequency band over 100 kHz of impedance signatures from tendon-anchorage of PSC girder (Kim *et al.* 2010)

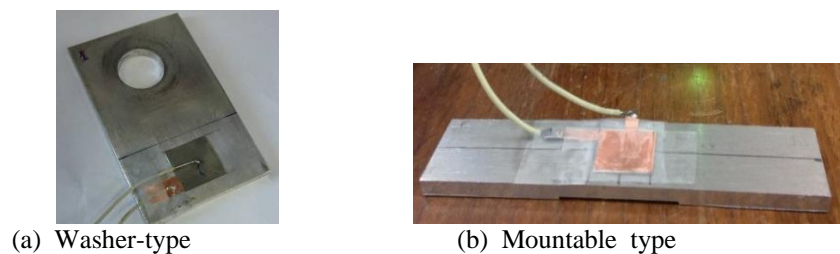


Fig. 9 Two types of PZT interfaces

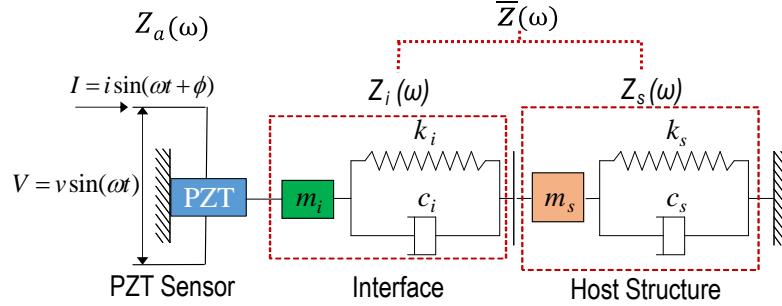


Fig. 10 PZT interface -host structure system (Huynh and Kim 2017b)

To overcome the limitation of the washer-type interface, Huynh and Kim (2014) proposed a mountable PZT interface which can be easily attached to and detached from the host structure, see Fig. 9(b).

For the theoretical feasibility of the interface technique, Huynh and Kim (2017b) proposed an EM impedance model to represent coupled dynamic responses of PZT interface-host structure, as shown in Fig. 10. The PZT interface-host structure is modeled as a spring-mass-damper system, in which m_i , c_i , k_i and m_s , c_s , k_s are the masses, damping coefficients, and spring stiffness of the interface and the host structure generated at the PZT driving point. In this 2-DOF system, one refers to the host structure represented by the impedance Z_s and the other refers to the interface represented by its impedance Z_i .

The SM (i.e., structural mechanical) impedance \bar{Z} of the interface-host structure system at the PZT driving point is defined as the ratio between the excitation force F_i and the velocity \dot{x}_i , as follows (Huynh and Kim 2017b)

$$\bar{Z}(\omega) = \frac{F_i}{\dot{x}_i} = \frac{K_{11}K_{22} - (K_{12})^2}{i\omega K_{22}} \quad (7)$$

in which, the terms $[K_{ij}]$, $i, j = 1, 2$ are the dynamic stiffness of the 2-DOF system, as follows:

$$\begin{bmatrix} K_{11} & K_{12} \\ K_{12} & K_{22} \end{bmatrix} = \begin{bmatrix} -\omega^2 m_i + i\omega c_i + k_i & -i\omega c_i - k_i \\ -i\omega c_i - k_i & -\omega^2 m_s + i\omega(c_i + c_s) + (k_i + k_s) \end{bmatrix} \quad (8)$$

By substituting Eq. (8) into Eq. (7), the resultant EM impedance response of the 2-DOF model of the PZT interface-host structure system can be obtained, as follows:

$$Z(\omega) = \left\{ i\omega \frac{w_a l_a}{t_a} \left[\hat{\epsilon}_{33}^T - \frac{1}{Z_a(\omega)/\bar{Z}(\omega) + 1} d_{31}^2 \hat{Y}_{11}^E \right] \right\}^{-1} \quad (9)$$

The 2-DOF impedance model contains two resonant peaks in its impedance signatures which represent the two coupled vibration modes of the PZT interface-host structure system. Since the 2-DOF impedance model represents the structural parameters of both the interface device and the host structure, any structural changes occurred in the host structure (or the PZT interface) can result to the changes in the measured EM impedance signatures. Therefore, the structural integrity

of the host structure can be estimated by monitoring the impedance changes obtained from the PZT interface.

4.2 Impedance measurements via PZT interfaces

To demonstrate the feasibility of the PZT interface technique for impedance monitoring, Huynh and Kim (2017b) analytically investigated a simple example of the 2-DOF impedance model of the PZT interface-host structure system. The structural properties of the host structure are set as follows: $m_s = 1$ (kg), $c_s = 125$ ($N/m^{s^{-1}}$), $k_s = 5 \times 10^{10}$ (N/m) while those of the interface are selected as: $m_i = 0.2$ (kg), $c_i = 125$ ($N/m^{s^{-1}}$), $k_i = 1 \times 10^{10}$ (N/m). Material properties and geometric sizes of the PZT patch are as follows: $Y_{11}^E = 6.3 \times 10^{10}$ (N/m^2), $\rho = 7650$ (kg/m^3), $d_{31} = -1.66 \times 10^{-10}$ (m/V), $\epsilon_{33}^T = 1.5 \times 10^{-8}$ (Farads/m), $\delta = 0.005$, $\eta = 0.001$, $w_a = 25.4$ (mm), $t_a = 0.254$ (mm) $l_a = 25.4$ (mm). The structural changes in the host structure are simulated by sequentially reducing its spring stiffness k_s up to 10%, 20%, and 30%. Fig. 11 shows the impedance signatures of the EM model under various stiffness reductions in the host structure. As observed in the figure, there exist two impedance peaks corresponding to the two vibration modes of the 2-DOF impedance model. The first impedance peak has relatively higher magnitude than the second one. It is found that the change in the host structure's stiffness causes the decrease in the resonant frequencies. Note that the impedance peaks represent the significant contributions of the SM impedance to the EM impedance.

Nguyen *et al.* (2011) used the washer-type interface for bolt-loosening monitoring in the bolted connections. As shown in Fig. 12(a), the PZT interfaces were inserted into the bolt joints to monitor the change in the bolt torque. The change in the bolt torque would modify the boundary condition of the PZT interface resulting in the variation of the impedance responses. The bolt-torque was set at 160 N.m as intact case and four levels of torque-loss were considered. The impedance measurements showed that resonant impedance responses occurred below 100 kHz and they were sensitively varied with the bolt-loosening in the connection, see Fig. 12(a).

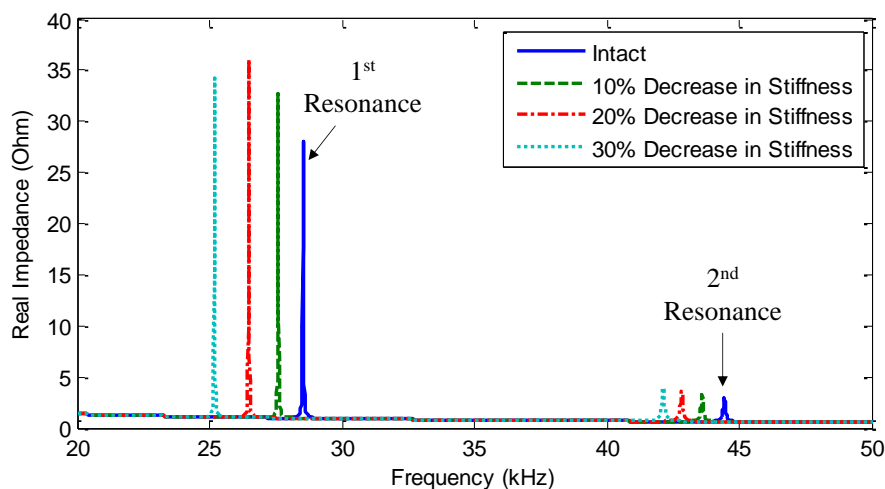


Fig. 11 Impedance signatures of 2-DOF impedance model (Huynh and Kim 2017b)

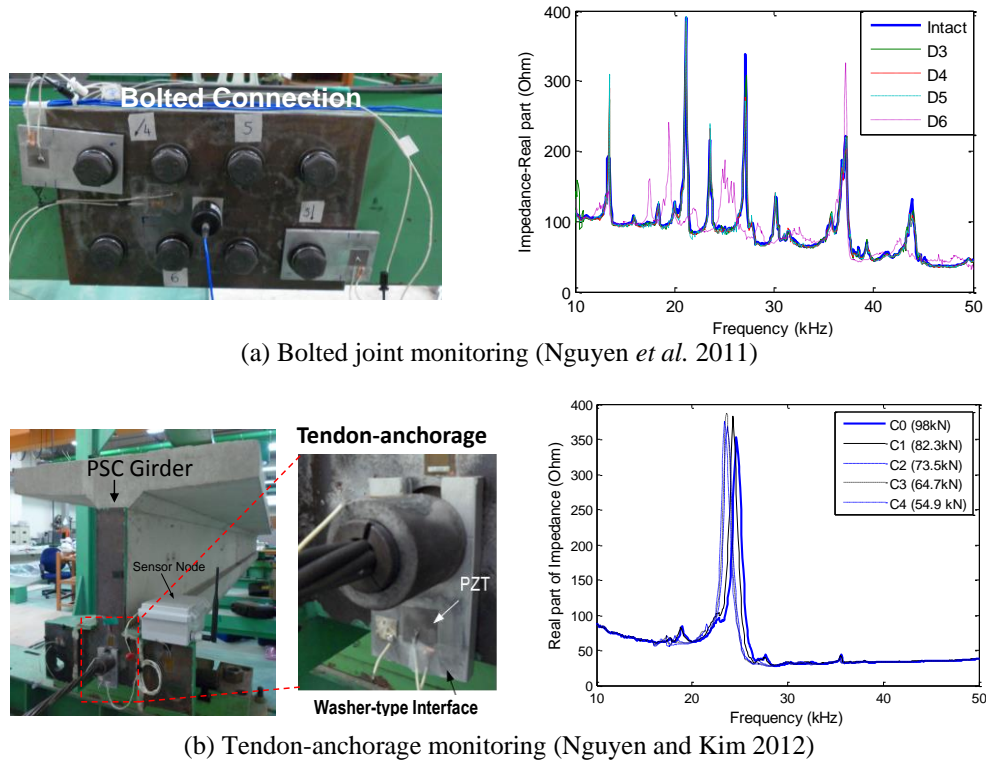
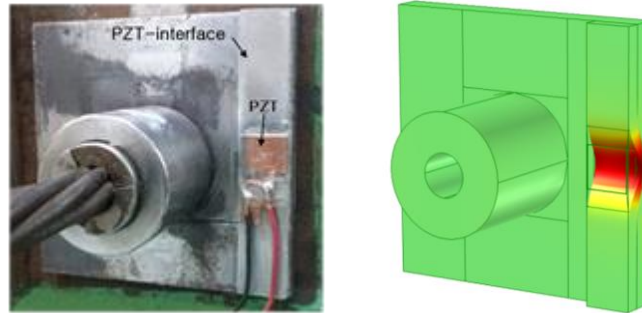


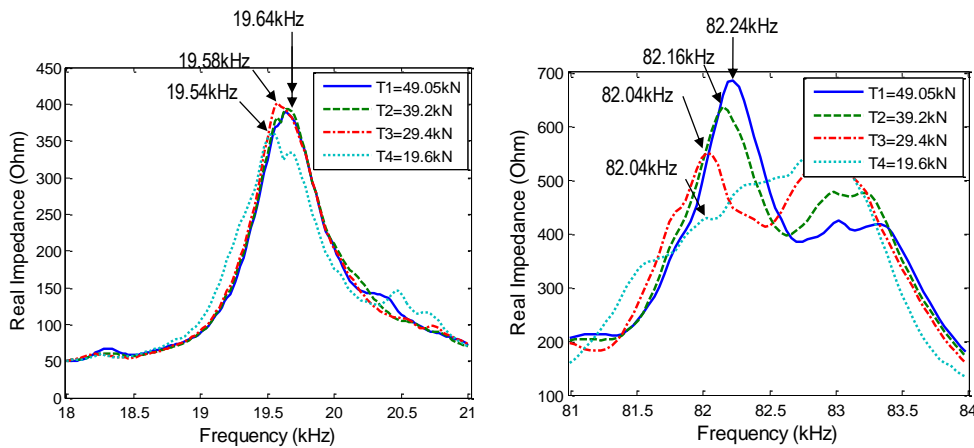
Fig. 12 Sensitive frequency range below 100 kHz of impedance signatures via washer-type interface

By using the same methodology, Nguyen and Kim (2012) inserted the PZT interface washer into the joint between the anchor block and the bearing plate of a PSC girder to monitor the prestress-loss, as shown in Fig. 12(b). For various prestress levels of the PSC girder, the impedance responses were wirelessly measured by using the smart impedance sensor nodes SSeL-I. The experimental results demonstrated that the interface washer technique predetermined resonant impedance peaks below 100 kHz and thus reduced the need of high-performance impedance analyzers (e.g., HIOKI-3532 or HP4194A). Also, the resonant impedance response was shifted to the left as the prestress force was reduced from 98 kN to 54.9 kN. The reduction in the resonant frequency indicated the loss of the modal stiffness of the tendon-anchorage system.

Huynh and Kim (2014) evaluated the performance of the mountable PZT interface for a cable system. The interface was surface-mounted on the bearing plate of the cable-anchorage connection to monitor the change in the prestress force, as shown in Fig. 13(a). The local dynamic response of the PZT interface at resonance is also shown in the figure. The impedance responses were recorded by a wired impedance sensing system HIOKI-3532 for different levels of prestress force. The change in the prestress force would modify the stress field and boundary condition of the connection, leading to the variation of the dynamic response of the PZT interface; as the result, the impedance signatures is altered. Figure 13(b) shows the impedance responses in two effective frequency ranges below 100 kHz. It is observed that these impedance responses were verified sensitively as the prestress force was reduced from 49.05 kN to 19.6 kN.



(a) Tendon-anchorage with mountable interface and local dynamic response



(b) Sensitive impedance responses

Fig. 13 Sensitive frequency range below 100 kHz of impedance signatures via mountable interface (Huynh and Kim 2014)

5. Compensation of temperature effects on impedance monitoring

5.1 Effects of temperature variation

Temperature effects have been regarded as one of the most critical issues that have hindered the application of the EM impedance technique to real structures. The temperature variation can modify the piezoelectric properties of the sensor and the dynamic characteristics of the monitored structure. As described in Eq. (3), the overall EM impedance of the PZT-host structure system is a function of the piezoelectric properties of the PZT sensor and the dynamic properties of the host structure. The contribution of the PZT sensor to the overall EM impedance is represented by the dielectric constant (ϵ_{33}^T), the coupling constant (d_{31}), the Young's modulus (Y_{11}^E) of the PZT material and the sensor's geometric parameters (w_a , l_a , and t_a). It is known that the piezoelectric properties of the PZT sensor vary with temperature. Figure 14 shows the variation of the dielectric constant and the coupling constant of typical piezoelectric materials (PZT-5A and PZT-5H) due to

the temperature change (Piezo Systems 2011). Both the dielectric constant and the coupling constant vary proportionally with the temperature and they are dependent on the type of piezoelectric materials. The Young's modulus and the PZT sensor's size are also reported as temperature-dependent parameters (Hooker 1998, Park *et al.* 1999). Among the above temperature-dependent parameters, the dielectric constant exhibits the most significant effect on the electrical impedance of the PZT sensor (Park *et al.* 1999).

The contribution of the host structure to the overall EM impedance is determined by the SM impedances (Z_s). It is noted from Eq. (4) that the SM impedance Z_s is directly associated with the dynamic properties of the monitored structure (m_s, c_s, k_s). It is reported that the temperature has influences on the dynamic properties of structures (Woon and Mitchell *et al.* 1996, Kim *et al.* 2003, Sohn 2007, Huynh *et al.* 2015c). The Young's modulus of a structure varies slightly with the temperature and the thermal expansion of the material will induce stresses in constrained structures. Park *et al.* (1999) examined temperature effects on dynamic responses of a steel beam structure at high frequencies and they showed that an increase in temperature leads to shifting of resonant frequencies and fluctuations in resonant response magnitudes. Obviously, the dynamic properties of the host structure monitored by the impedance-based technique are changed due to the temperature variation.

Fig. 15 illustrates the variation of the overall EM impedance signatures obtained from a PZT-aluminum beam under the temperature changes (Fabricio *et al.* 2014). It is shown that the peak frequencies and their amplitudes shifted toward the left as the temperature was increased; the higher frequency ranges exhibited the more significant shifts in impedance peaks and their magnitudes than the lower ones. Because the damage quantification has relied on statistically comparing the two impedance signals obtained at different times, the temperature effects can cause the unwanted changes in the damage indices, leading to the false damage detection.

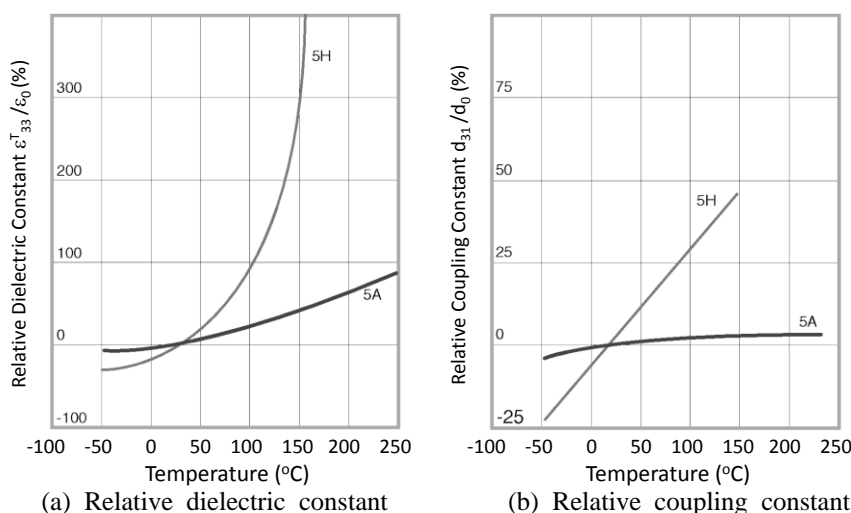


Fig. 14 Variation of dielectric constant and coupling constant of typical PZT materials due to temperature change (Piezo Systems 2011)

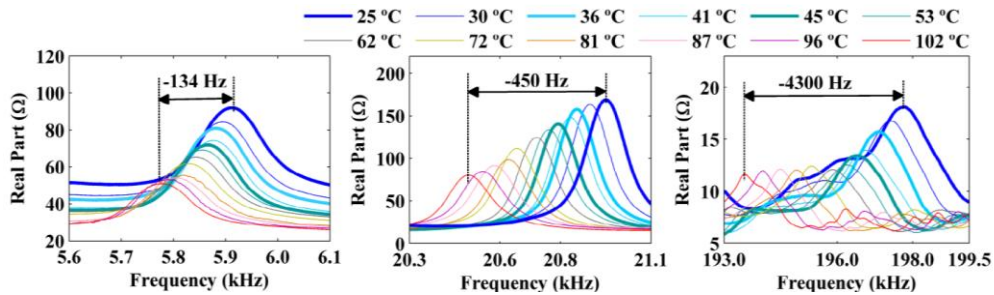


Fig. 15 Temperature effects on impedance signatures of a PZT-aluminum beam (Fabricio *et al.* 2014)

The effects of temperature variation and damage on the impedance responses were investigated for the tendon anchorage of a PSC girder by the authors (Huynh and Kim 2016). The mountable PZT interface technique was utilized to acquire the impedance responses of the tendon anchorage. Experimental analyses revealed that the impedance features (e.g., peak frequency, peak magnitude, RMSD, CCD) of the tendon anchorage changed nonlinearly with the temperature and prestress force. The lower frequencies exhibited the higher variations in the impedance features. The numerical examination showed the variation of the stress field of the tendon anchorage under the effects of prestress force and temperature variation (Huynh and Kim 2017a). Under prestressing, the tendon anchorage is deformed and this deformation caused changes in the stress field of the PZT interface, see Fig. 16(a). These stress fields can be further changed when the tendon anchorage system experienced temperature variation, see Fig. 16(b). These stress field changes induced the variation of the impedance responses of the tendon anchorage, see Fig. 17. Their further investigation explained the mechanism of the temperature variation effect via the dual effects on the impedance responses. As the temperature was increased, the tendon was relaxed by losing its tension, resulting in the softening effect. At the same time, the local compressive stress was built up at the bonded sections of the PZT interface, resulting in the local stiffening effect. The greater stiffening effect in the tendon anchorage system increased the resonant frequencies of impedance peaks, see Fig. 17(b).

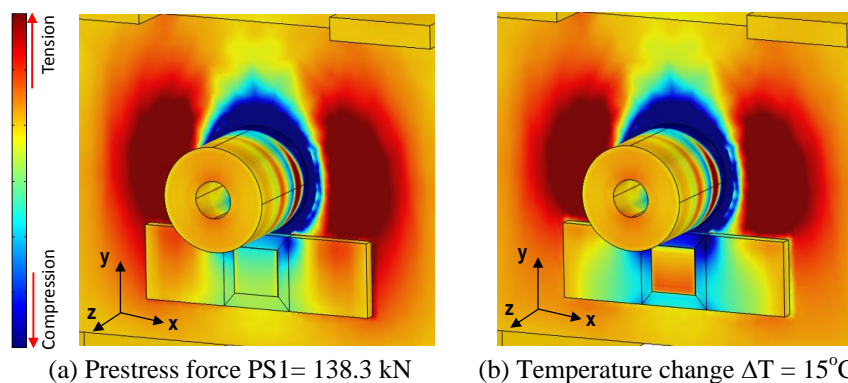


Fig. 16 Tendon anchorage's stress fields in x-direction under effects of prestress force and temperature variation (Huynh and Kim 2017a)

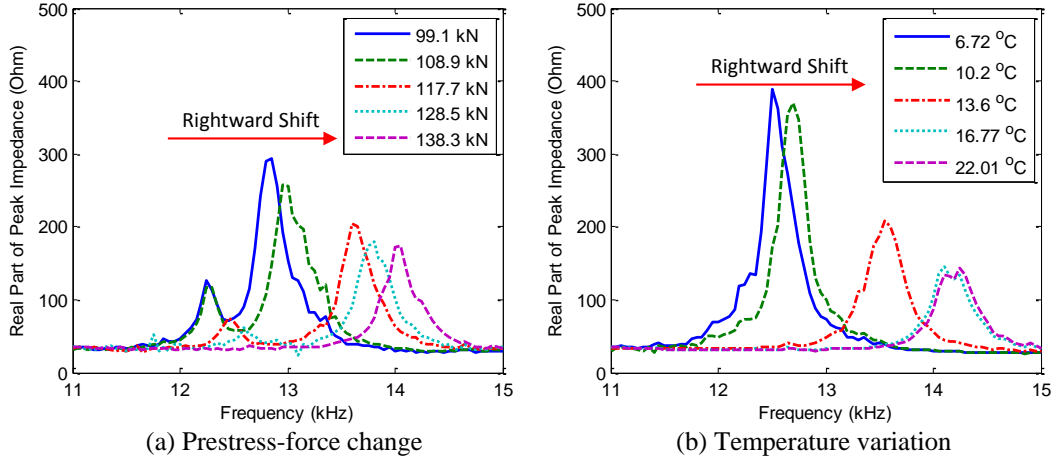


Fig. 17 Shifts of impedance peaks of tendon anchorage due to temperature variation and prestress-force change (Huynh and Kim 2017a)

5.2 Temperature-effect compensation

Several compensation methods of temperature effect based on pattern recognition algorithms and soft computing techniques were developed for the impedance-based damage detection. Park *et al.* (1999) compensated the temperature effects by correcting the measured impedance $\text{Re}(Y_j)_{\text{measured}}$ using an introduced parameter δ^s , which is the average difference between reference impedance and measured impedance, as follows

$$\text{Re}(Y_j) = \text{Re}(Y_j)_{\text{measured}} + \delta^s \quad (10)$$

By taking the advantage that the variation in impedance is dominated by horizontal shifts of impedance peaks, the frequency shift and parameter δ^s can be obtained by iteration searching for the minimum value of the damage metric. To minimize the temperature effects on the piezoelectric material itself, their study suggested that the impedance-based technique should utilize the real part of the EM impedance for detecting the structural integrity.

Based on the Park's work, Koo *et al.* (2009) proposed an effective frequency shift (EFS)-based statistical algorithm to compensate the temperature effect. The idea is based on estimating the required frequency shift to achieve the maximum cross-correlation coefficient (i.e., maxCC index) between the baseline and the current impedance. For the intact state under temperature variation, the temperature change (δT) causes approximately the same frequency shift ($\delta\omega_{\delta T}$) for each impedance peak, see Fig. 18(a). Meanwhile, the damage state under temperature change induces the coupled frequency shift ($\delta\omega_{d+\delta T}$), see Fig. 18(b). After the EFS compensation, the temperature effects are filtered from the impedance signatures and the CCD_{EFS} index could be much more significant to indicate the damage state. The Koo's technique was applied to compensate the temperature effects on the impedance signals of a lab-scaled critical member of Seongsu Bridge

(Korea). Since Koo’s technique requires simple computations and can be utilized for general impedance-based applications, it has continued to be used in recent damage detection jobs (Yun *et al.* 2013, Siebel and Lilov 2013, Huynh and Kim 2016). Rabelo *et al.* (2017) utilized the EFS analysis as the temperature-compensation technique to determine threshold-level for health monitoring of panels under varying temperature.

Huynh and Kim (2017a) compensated temperature effects on the impedance responses of the tendon anchorage via the EFS-based method. In their study, the impedance responses of the tendon anchorage were monitored under the temperature variation (6.72-22.33°C) and the different prestress levels (PS1 = 138 kN, PS1 = 129 kN, PS1 = 118 kN, PS1 = 109 kN, PS1 = 99 kN), as shown in Fig. 19. It is observed from Figs. 19(a) and 19(b), the excellent match between two impedance signatures of the tendon anchorage at different temperatures (22.33°C vs 6.72°C) was obtained after the EFS. Before the EFS (Fig. 19(a)), a considerable CCD value, 56.6%, can be observed between two impedance signatures. After the EFS (Fig. 19(b)), the CCD value was significantly reduced to 2.9%, indicating the effective compensation of the temperature effects. As shown in Fig. 19(c), after the EFS-based temperature compensation, the CCD was very small for the intact case, but significant when the damage (i.e., prestress-loss events PS1-PS5) occurred in the tendon anchorage. However, an issue of the EFS-based technique is on selecting the frequency range which should be sensitive to damage but sufficiently narrow for the temperature compensation. In their study, to enhance the accuracy of the damage detection, Huynh and Kim (2017a) used multiple narrow frequency ranges for the EFS-based temperature compensation and the damage quantification.

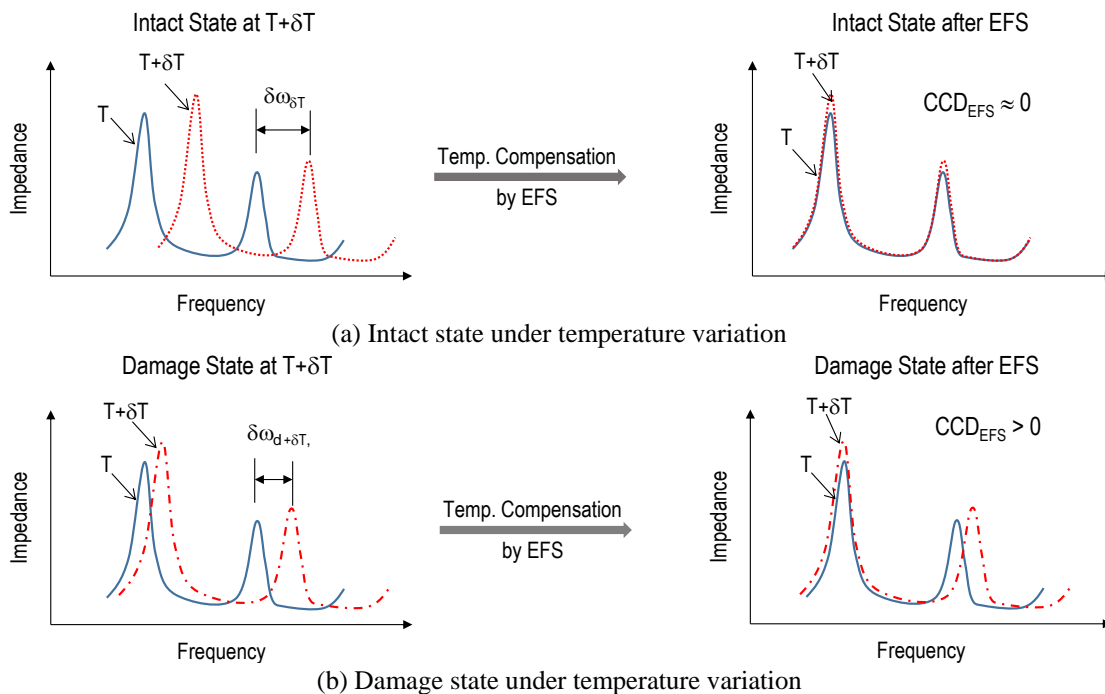


Fig. 18 EFS-based temperature compensation method

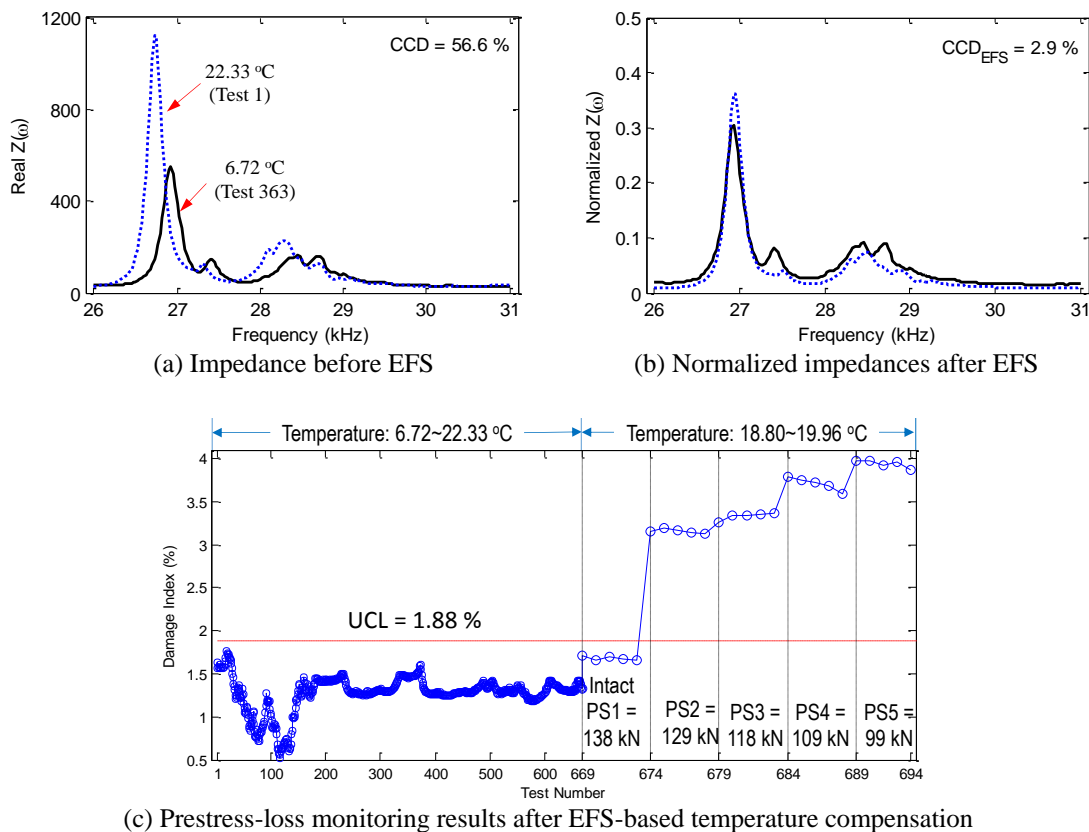


Fig. 19 EFS-based temperature compensation for impedance signatures of tendon anchorage (Huynh and Kim 2017a)

Tibaduiza *et al.* (2013) and Min *et al.* (2015) have applied the principal component analysis (PCA) to compensate the experimental uncertainties such as noise, redundancies, and temperature effects for impedance-based damage detection jobs. The PCA technique is regarded as a simple and nonparametric statistical technique which is used to emerge the variation and bring out the strong patterns in a high-dimensional data. The PCA technique linearly transforms an original dataset of variables into a substantially smaller one of uncorrelated variables which can describe most of the information of the original dataset. This technique has been used in a wide variety of engineering problems because it often makes the dataset easier to explore and visualize. By searching the governing trends that represent the original dataset, the unwanted noises could be filtered out of the complex data via the processes of data compression and information extraction. Lim *et al.* (2011) has proposed a data normalization technique based on the Kernel PCA to minimize false-alarms caused by varying temperature and external loading conditions, as shown in Fig. 20. The Kernel PCA is recognized as a nonlinear PCA that searches for a nonlinearly transformed high dimensional space. The Kernel PCA-based technique showed effectiveness in detect bolt-loosening in a metal connection of a composite aircraft wing under temperature and loading variations (Lim *et al.* 2011).

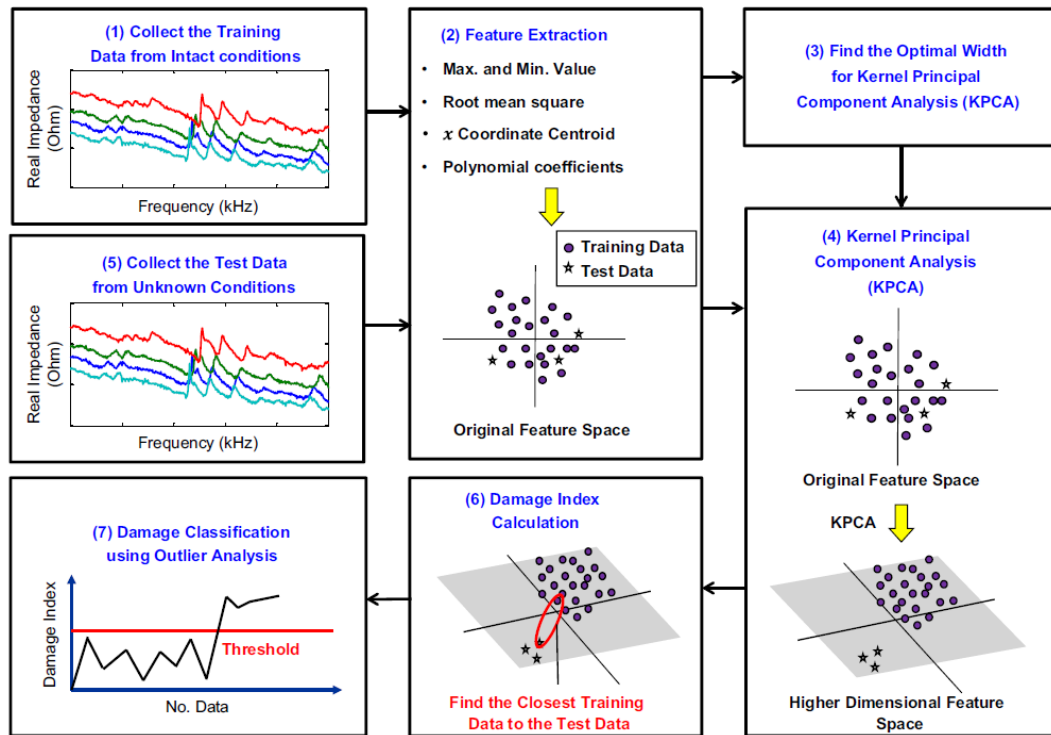
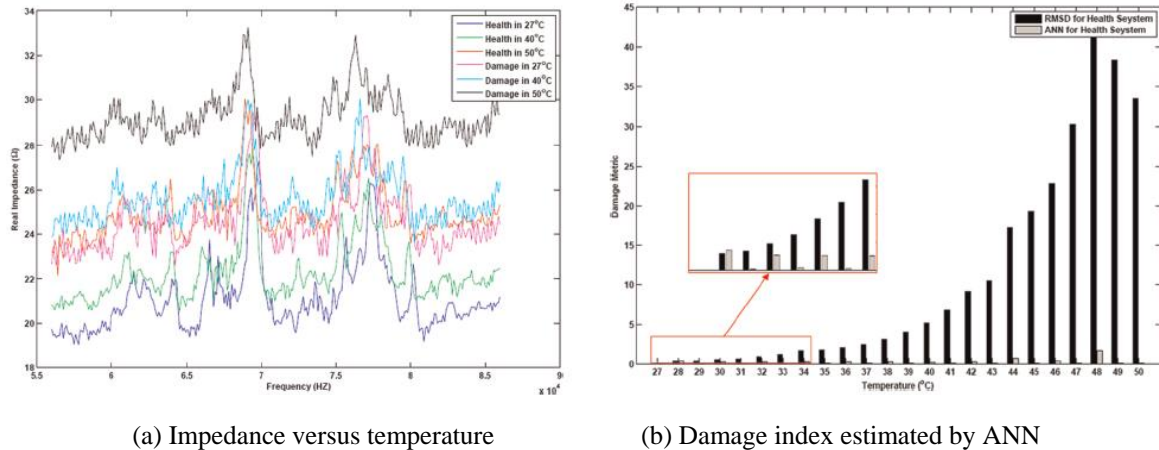


Fig. 20 Data normalization technique using Kernel PCA (Lim *et al.* 2011)

A soft computing technique is an alternative and innovative tool to filter the temperature-induced variation in impedance signatures. Artificial neural network (ANN) has been previously applied for various impedance-based damage detection practices. Lopes *et al.* (2000) implemented the ANN to quantitatively estimate the damage in structures via impedance responses. Giurgiutiu and Zagrai (2005) classified the near-field and medium-field spectra for high-frequency impedance-based damage detection. Also, Min *et al.* (2010) determined a properly-narrow frequency band of impedance responses by using the ANN. Sepehry *et al.* (2011) proposed the ANN-based temperature compensation procedure to minimize the temperature-induced variation in impedance measurements. Yang *et al.* (2015) used the radial basis function network (RBFN), which is a particular type of the ANN using radial basis functions (RBFs) as activation functions, to eliminate the noise caused by the external force on the impedance monitoring. To filter out the effect of the external force, impedance signatures corresponding to a particular force condition were estimated by the RBFN-based regression analysis. Fig. 21 shows the ANN-based temperature-effect compensation for the impedance monitoring in bolted joints (Sepehry *et al.* 2011). In their study, it is observed that with a proper training dataset, the ANN-based method can significantly compensate the temperature effects. For most ANN-based algorithms, acquiring appropriate training data from in-situ structures under damaged states is a challenging job unless the structures are well modeled via finite element analysis.



(a) Impedance versus temperature

(b) Damage index estimated by ANN

Fig. 21 Temperature compensation by RBFN-based method (Sepehry *et al.* 2011)

6. Discussions on future challenges

In spite of the recent research efforts, there exist important issues that should be addressed for successful implementations of the impedance-based SHM technique for civil structures. At least six major issues are raised as follows: (1) applicability of wireless impedance sensors, (2) predetermination of effective frequency band, (3) sensing region of impedance signatures, (4) robust compensation of temperature and noise effects, (5) quantitative estimation of damage severity, and (6) long-term durability of sensors.

6.1 Applicability of wireless impedance sensors

Up-to-date, the design of wireless impedance sensor nodes have been relied on the low-cost impedance chip AD5933 which has the measurable frequency range only within 1-100 kHz (Analog Devices 2010). In many cases, however, the EM impedance signal is required to be measured in higher frequency ranges in order to sensitively capture small-size of damage. For examples, effective frequency bands over 100 kHz were obtained from steel brackets of the airplane (Chaudhry *et al.* 1995), concrete bridge (Soh *et al.* 2000) and prestressed tendon-anchorage (Kim *et al.* 2010). For the target structures whose effective frequency ranges can be over 100 kHz, a high-performance, high-cost and bulky-size impedance analyzer is needed. Therefore, future research efforts are needed to expand the measurable frequency range of the wireless impedance sensor nodes.

Also, the long-term reliability of the hardware and software of the wireless impedance sensor nodes is another issue. So far, there has been very little research that examines the long-term performance of the wireless impedance sensor networks. For field applications, there are many problems need to be solved to achieve successful wireless impedance-based SHM. These key issues include energy harvesting (energy saving and self-powering), bandwidth and frequency of wireless transmission, real-time ability, on-board computation, and integration of the wireless impedance nodes to the multi-scale sensing network.

6.2 Predetermination of effective frequency band

In impedance monitoring practices, the determination of effective frequency bands is a target-dependent problem. To sense incipient-type damage, the effective frequency range is typically ranged from 30 kHz to 250 kHz (Stokes and Clouds 1993). For most cases, the effective frequency ranges are unknown and traditionally identified by the try-and-error method. Park *et al.* (2003) reported that frequency ranges higher than 200 kHz are found to be suitable for local sensing regions while the ones lower than 70 kHz can deal with a larger sensing area. Min *et al.* (2010) have proposed a scheme using artificial neural networks (ANNs) for autonomously selecting effective frequency ranges within measured impedance signatures. As with the ANNs, it is hard to acquire suitable training patterns unless target structures can be accurately modeled for finite element analyses.

The PZT interface technique can be considered as a promising way to predetermine the effective frequency bands in impedance monitoring practices (Park 2009, Nguyen *et al.* 2011, Nguyen and Kim 2012). However, most of PZT interfaces are target-oriented devices that have been designed particularly tailored to prestressed joints such as tendon-anchorage or bolted connections. Thus, there still exists a need to design an alternative interface device that is suitable for target-free applications.

6.3 Sensing region of impedance responses

The sensing range of impedance signatures is important for the proper sensor placement on the target structure. At high-frequency ranges, the sensing region of the piezoelectric sensor is localized to a small region, which is close to the sensor. Because of the limited sensing area, the impedance signatures is affected only by the changes in the structural properties close to the sensor (Chaudhry *et al.* 1995).

So far, there has been very little research on determining the sensor's sensing region for the impedance-based method. Esteban (1996) conducted theoretical modeling efforts based on the wave propagation approach to identify the PZT's sensing region. Based on the knowledge acquired via various case studies, Park *et al.* (2000) reported that depending on the material and density of the structure the sensing area of a single PZT can vary anywhere from 0.4 m on composite reinforced concrete structures to 2 m on simple metal beams. Hu and Yang (2007) conducted a fundamental research work of determining the PZT sensing region based on the wave propagation modeling; however, the theoretical development was limited to thin beam-like specimens. Thus, intensive studies on the sensing region of impedance responses still remain in the future.

6.4 Robust compensation of temperature and noise effects

Real structures exist in an environment of ambient conditions that can cause uncertainties in impedance monitoring and decision-making. As reviewed previously, there exist at least three well-known algorithms to compensate the temperature effects on impedance signatures (Huynh 2017). These include: the PCA-based method (Lim *et al.* 2011, Tibaduiza *et al.* 2013, and Min *et al.* 2015), the network-based method (Sepehry *et al.* 2011 and Yang *et al.* 2015), and the EFS-based method (Koo *et al.* 2009, Huynh and Kim 2016). The accuracy of the PCA-based algorithm depends upon the selection of the principal components which are significantly affected by the temperature variation relative to the structural damage. The accuracy of the network-based

algorithm is dependent on the selection of damage features to train and the number of training datasets. The issue of the EFS-based method is on selecting the frequency range which should be sensitive to damage but sufficiently narrow for the temperature compensation. For real implementations, there is a need to evaluate the robustness of the temperature compensation methods. Thus, the performance of the well-known algorithms is needed to be comparatively examined.

Noises induced by the effect of external loads should be compensated carefully in practical applications of the impedance-based technique. The external load would induce additional stress into the monitored structure causing the variation of the impedance baseline. Lim and Soh (2012) experimentally showed that the peaks of admittance signatures shifted progressively to the right with the increment in tensile/compressive forces. Lim *et al.* (2011) used a data normalization technique to enhance the impedance-based damage detection under the condition of external loadings. Yang *et al.* (2015) have proposed an ANN-based technique to compensate tensile force's effects on impedance signatures.

The vibration of the host structure could also cause external excitations on the EM impedance signatures obtained from PZT sensors. Yang and Miao (2010) concluded that the influence of external excitations on the EM impedance signatures can be ignored when the external frequency is much smaller or much higher than the PZT scanning frequency. Priya *et al.* (2014) showed that the low-frequency vibration of the host structure has ignorable effects on the impedance signatures obtained from PZT sensors. Unlike the effect of external loads, the mechanism of the effect of external excitations on the impedance responses has not fully studied due to the difficulties in dealing with high-frequency components. More research effort is still needed to better understand the mechanism of the external excitation effect.

6.5 Quantification estimation of damage severity

Despite the impedance-based technique has been successfully implemented on various types of structures, the quantitative damage detection by the impedance-based technique has become a critical issue, especially for the complex structural connections. Since the impedance technique is not based on any particular physical models, it is very difficult to correlate the change in impedance signatures with the change in structural properties. As the result, the technique can only provide limited information on the nature of the damage.

Ritdumrongkul *et al.* (2004) attempted to estimate the damage severity of a bolted joint using measured impedance signatures and a mathematical optimization. However, the frequency band considered in their study was relatively low, less than 2.5 kHz, as compared to the ones commonly used in real applications. Lopes *et al.* (2000) and Min *et al.* (2012) proposed the impedance-based technique combining with the ANNs for the identification of damage severity in structural connections. Huynh and Kim (2017b) attempted to quantitatively estimate the prestress-loss severity in the tendon anchorage by using the impedance signatures and model updating. So far, there have been very few research studies reported on the quantitative health monitoring using the impedance signatures. Thus, quantitative damage estimation in the impedance-based technique still remains challenging.

6.6 Long-term durability of sensors

Most of the piezoelectric sensors are brittle. Therefore, the fracture and functional degradation

of the sensors should be confirmed for the successful impedance monitoring (Giurgiutiu 2014). Giurgiutiu *et al.* (2002) reported that as the debonding severity of the sensor increases, the resonant impedance peaks becomes sharper and more distinctive while the resonance magnitudes of the host structure decreases. To minimize the influence of the bonding layers, Bhalla and Soh (2004) recommended an adhesive with high shear modulus and thin thickness, and small-sized piezoelectric sensors should be used. Park *et al.* (2006) proposed a piezoelectric sensor-diagnostic process by tracking the imaginary part (susceptance) of the measured admittance signatures. Park *et al.* (2008) modified an EM impedance model for sensor diagnostics with the considerations of the sensor quality assessment and coupling degradation effects.

So far, the durability of the piezoelectric sensors has not extensively evaluated, especially under long periods in the order of years. In real-life target structures such as buildings, bridges, machine parts, aerospace systems that can expose the harsh environment, it is very difficult to maintain the bonding condition and the functionality of the sensors. Because the consistent behavior of the sensors plays an essential role in achieving a successful decision-making of damage occurrence, the protection approach that can protect the sensor from the harsh environment should be developed.

7. Conclusions

In this paper, current advances and future challenges of the impedance-based structural health monitoring were presented. Firstly, theoretical background of the impedance-based method was outlined. Next, an overview was given to recent advances in the wireless impedance sensor nodes, the interfacial impedance sensing devices, and the temperature-effect compensation algorithms. Various research works on these topics were reviewed to share up-to-date information on research activities and implementations of the impedance-based technique. Finally, future research challenges of the technique were discussed including the applicability of wireless sensing technology, the predetermination of effective frequency bands, the sensing region of impedance responses, the robust compensation of noise and temperature effects, the quantification of damage severity, and long-term durability of sensors.

Acknowledgments

This work was supported by a Research Grant of Pukyong National University (2016 year).

References

- Analog Devices (2010), "Datasheet of AD5933", <http://www.analog.com>
- Annamdas, V.G.M., (2012), "Facts of piezo impedance technique in crack propagation studies for an engineering structure", *Int. J. Aerosp. Sci.*, **1**(2), 8-15.
- Ayres, J.W., Lalande, F., Chaudhry, Z. and Rogers, C.A. (1998), "Qualitative impedance-based health monitoring of civil infrastructures", *Smart Mater. Struct.*, **7**, 599-605.
- Balageas, D., Fritzen, C.P. and Gueemes, A. (2006), "Structural health monitoring", Wiley-ISTE.
- Bhalla, S. and Soh, C.K. (2004), "Electromechanical impedance modeling for adhesively bonded piezo-transducers", *J. Intel. Mat. Syst. Str.*, **15**(12), 955-972.

- Bilgunde, P. and Bond, L.J. (2017), "Temperature dependence of electromechanical impedance based bond-line integrity monitoring", *Proceeding of SPIE*, 10170, 1-11.
- Burgoyne, C.J. and Scantlebury, R.C. (2008), "Lessons learned from the bridge collapse in Palau", *Proceeding of the Institution of Civil Engineers: Civil Engineering*, 161, 28-34.
- Chaudhry, Z., Joseph, T., Sun, F. and Rogers, C. (1995), "Local-area health monitoring of aircraft via piezoelectric actuator/sensor patches", *Smart Structures and Integrated Systems, Proceedings of the SPIE*, 2443, San Diego, CA.
- Fabricio G.B., Danilo E.B., Vinicius A.D.A. and Jose A.C.U. (2014), "An experimental study on the effect of temperature on piezoelectric sensors for impedance-based structural health monitoring", *Sensors*, **14**, 1208-1227.
- Giurgiutiu, V. (2014), *Structural health monitoring with piezoelectric wafer active sensors*, 2nd Ed., Academic Press.
- Giurgiutiu, V. and Zagrai, A. (2002), "Embedded self-sensing piezoelectric active sensors for on-line structural identification", *J. Vib. Acoust.*, **124**, 116-125.
- Giurgiutiu, V. and Zagrai, A. (2005), "Damage detection in thin plates and aerospace structures with the electro-mechanical impedance method", *Struct. Health Monit.*, **4**(2), 99-118.
- Ho, D.D., Ngo, T.M. and Kim, J.T. (2014), "Impedance-based damage monitoring of steel column connection: numerical simulation", *Struct. Monit. Maint.*, **1**(3), 339-356.
- Ho, D.D., Lee, P.Y., Nguyen, K.D., Hong, D.S., Lee, S.Y., Kim, J.T., Shin, S.W., Yun, C.B. and Shinozuka, M. (2012), "Solar-powered multi-scale sensor node on imote2 platform for hybrid SHM in cable-stayed bridge", *Smart Struct. Syst.*, **9**(2), 145-164.
- Hooker, M.W. (1998), "Properties of PZT-based piezoelectric ceramics between -150 and 250°C", *Technical Report NASA/CR-1998-208708*, NASA, USA
- Hou, J., Jankowski, L. and Ou, J. (2014), "Structural health monitoring based on combined structural global and local frequencies", *Math. Problem. Eng.*, 1-13.
- Hu, X., Zhu, H. and Wang, D. (2014), "A study of concrete slab damage detection based on the electromechanical impedance method", *Sensors*, **14**, 19897-19909.
- Hu, Y. and Yang, T. (2007), "Wave propagation modeling of the PZT sensing region for structural health monitoring", *Smart Mater. Struct.*, **16**, 706-716.
- Huynh, T.C. (2017), "Wireless impedance-based structural health monitoring of civil structures using smart PZT interface technique", *PhD Dissertation*, Pukyong National University, Korea.
- Huynh, T.C. and Kim, J.T. (2014), "Impedance-based cable force monitoring in tendon-anchorage using portable PZT-interface technique", *Math. Problem. Eng.*, 1-11.
- Huynh, T.C. and Kim, J.T. (2016), "Compensation of temperature effect on impedance responses of PZT interface for prestress-loss monitoring in PSC girders", *Smart Struct. Syst.*, **17**(6), 881-901.
- Huynh, T.C. and Kim, J.T. (2017a), "Quantification of temperature effect on impedance monitoring via PZT interface for prestressed tendon anchorage", *Smart Mater. Struct.*, **26**(12), 1-19.
- Huynh, T.C. and Kim, J.T. (2017b), "Quantitative damage identification in tendon anchorage via PZT interface-based impedance monitoring technique", *Smart Struct. Syst.*, **20**(2), 181-195.
- Huynh, T.C., Lee, K.S. and Kim, J.T. (2015a), "Local dynamic characteristics of PZT impedance interface on tendon anchorage under prestress force variation", *Smart Struct. Syst.*, **15**(2), 375-393.
- Huynh, T.C., Nguyen, T.C., Choi, S.H. and Kim, J.T. (2016), "Impedance monitoring at tendon-anchorage via mountable PZT interface and temperature-effect compensation", *Proceedings of SPIE*, 9799, 1-6.
- Huynh, T.C., Park, J.H. and Kim, J.T. (2016b), "Structural identification of cable-stayed bridge under back-to-back typhoons by wireless vibration monitoring", *Measurement*, **88**, 385-401.
- Huynh, T.C., Park, Y.H., Park, J.H. and Kim, J.T. (2015b), "Feasibility verification of mountable PZT-interface for impedance monitoring in tendon-anchorage", *Shock Vib.*, 1-11.
- Huynh, T.C., Park, Y.H., Park, J.H., Hong, D.S. and Kim, J.T. (2015c), "Effect of temperature variation on vibration monitoring of prestressed concrete structures", *Shock Vib.*, 1-9.
- Kim, J.T., Huynh, T.C. and Lee, S.Y. (2014), "Wireless structural health monitoring of stay cables under two consecutive typhoons", *Struct. Monit. Maint.*, **1**(1), 47-67.

- Kim, J.T., Nguyen, K.D. and Huynh, T.C. (2013), "Wireless health monitoring of stay cable using piezoelectric strain response and smart skin technique", *Smart Struct. Syst.*, **12**(3-4), 381-379.
- Kim, J.T., Park, J.H., Hong, D.S. and Park, W.S. (2010), "Hybrid health monitoring of prestressed concrete girder bridges by sequential vibration-impedance approaches", *Eng. Struct.*, **32**, 115-128.
- Kim, J.T., Park, J.H., Hong, D.S. and Ho, D.D. (2011), "Hybrid acceleration-impedance sensor nodes on Imote2-platform for damage monitoring in steel girder connections", *Smart Struct. Syst.*, **7**(5), 393-416.
- Kim, J.T., Yun, C.B. and Yi, J.H. (2003), "Temperature effects on frequency-based damage detection in plate-girder bridges", *J. KSCE*, **7**(6), 725-733.
- Koo, K.Y., Park, S.H., Lee, J.J., and Yun, C.B. (2009), "Automated impedance-based structural health monitoring incorporating effective frequency shift for compensating temperature effects", *J. Intel. Mat. Syst. Str.*, **20**, 367-377.
- Lee, S.B. (1996), "Fatigue failure of welded vertical members of a steel truss bridge", *Eng. Fail. Anal.*, **3**(2), 103-108.
- Liang, C., Sun, F.P. and Rogers, C.A. (1994), "Coupled electro-mechanical analysis of adaptive material - Determination of the actuator power consumption and system energy transfer", *J. Intel. Mat. Syst. Str.*, **5**, 12-20.
- Liang, C., Sun, F.P. and Rogers, C.A. (1996), "Electro-mechanical impedance modeling of active material systems", *Smart Mater. Struct.*, **5**(2), 171-186.
- Lim, H.J., Kim, M.K., Sohn, H. and Park, C.Y. (2011), "Impedance-based damage detection under varying temperature and loading conditions", *NDT&E Int.*, **44**, 740-750.
- Lim, Y.Y. and Soh, C.K. (2012), "Effect of varying axial load under fixed boundary condition on admittance signatures of electromechanical impedance technique", *J. Intel. Mat. Syst. Str.*, **23**(7), 815-826.
- Lopes, V., Park, G., Cudney, H.H. and Inman, D.J. (2000), "Impedance-based structural health monitoring with artificial neural networks", *J. Intel. Mat. Syst. Str.*, **11**, 206-214.
- Lynch, J.P., Sundararajan, A., Law, K.H., Kiremidjian, A.S., Kenny, T. and Carryer, E. (2003), "Embedment of structural monitoring algorithms in a wireless sensing unit", *Struct. Eng. Mech.*, **15**(3), 385-297.
- Mascarenas, D., Todd, M.D., Park, G. and Farrar, C.R. (2007), "Development of an impedance-based wireless sensor node for structural health monitoring", *Smart Mater. Struct.*, **16**(6), 2137-2145.
- Min, J., Park, S. and Yun, C.B. (2010), "Impedance-based structural health monitoring using neural networks for autonomous frequency range selection", *Smart Mater. Struct.*, **17**(6), 1-10.
- Min, J., Park, S., Yun, C.B. and Song, B. (2010), "Development of a low-cost multifunctional wireless impedance sensor node", *Smart Struct. Syst.*, **6**(5-6), 689-709.
- Min, J., Park, S., Yun, C.B., Lee, C.G. and Lee, G. (2012), "Impedance-based structural health monitoring incorporating neural network technique for identification of damage type and severity", *Eng. Struct.*, **39**, 210-220.
- Min, J., Yi, J.H. and Yun, C.B. (2015), "Electromechanical impedance-based long-term SHM for jacket-type tidal current power plant structure", *Smart Struct. Syst.*, **15**(2), 283-297.
- Nagayama, T. (2007), "Structural health monitoring using smart sensors", Ph.D. Dissertation, University of Illinois at Urbana-Champaign.
- National Transportation Safety Board (NTSB) (2008), "Highway accident report interstate 35W collapse over the Mississippi River Minneapolis, Minnesota, August 1, 2007". *National Transportation Safety Board*, NTSB/HAR-08/02, Washington, D.C.
- Nguyen, K.D. and Kim, J.T. (2012), "Smart PZT-interface for wireless impedance-based prestress-loss monitoring in tendon-anchorage connection", *Smart Struct. Syst.*, **9**(6), 489-504.
- Nguyen, K.D., Lee, S.Y., Lee, P.Y. and Kim, J.T. (2011), "Wireless SHM for bolted connections via multiple PZT-interfaces and Imote2-platformed impedance sensor node", *Proceedings of the ANCRiSST 2011*, Dalian, China, July 2011.
- Nguyen, T.C., Huynh, T.C., Yi, J.H. and Kim, J.T. (2017), "Hybrid bolt-loosening detection in wind turbine tower structures by vibration and impedance responses", *Wind Struct.*, **24**(4), 385-403.
- Park, G., Cudney, H. and Inman, D.J. (2000), "Impedance-based health monitoring of civil structural components", *J. Infrastruct. Syst. - ASCE*, **6**(4), 153-160.

- Park, G., Kabeya, K., Cudney, H. and Inman, D. (1999), "Impedance-based structural health monitoring for temperature varying applications", *JSME Int. J. Series A Solid Mech. Mater. Eng.*, **42**, 249-258.
- Park, G., Sohn, H., Farrar, C. and Inman, D. (2003), "Overview of piezoelectric impedance-based health monitoring and path forward", *Shock Vib. Digest*, **35**(6), 451-463.
- Park, J.H. (2009), "Development of autonomous smart sensor nodes for hybrid structural health monitoring of large structures", Ph.D. Thesis, PKNU, Korea.
- Park, J.H., Huynh, T.C. and Kim, J.T. (2015), "Temperature effect on wireless impedance monitoring in tendon anchorage of prestressed concrete girder", *Smart Struct. Syst.*, **15**(4), 1159-1175.
- Park, J.H., Kim, J.T., Hong, D.S., Mascarenas, D. and Lynch, J.P. (2010), "Autonomous smart sensor nodes for global and local damage detection of prestressed concrete bridges based on accelerations and impedance measurements", *Smart Struct. Syst.*, **6**(5), 711-730.
- Park, S., Park, G., Yun, C.B. and Farrar, C.R. (2008), "Sensor self-diagnosis using a modified impedance model for active sensing-based structural health monitoring", *Structural Health Monitoring*.
- Park, S., Shin, H.H. and Yun, C.B. (2009), "Wireless impedance sensor nodes for functions of structural damage identification and sensor self-diagnosis", *Smart Mater. Syst.*, **18**, 1-11.
- Perera, R., Perez, A., Garcia-Dieguez, M. and Zapico-Valle J.L. (2017), "Active wireless system for structural health monitoring applications", *Sensors*, **17**, 1-16.
- Piezo Systems (2011), <http://www.piezo.com>
- Priya, C.B., Reddy, A.L., Rao, G.V.R., Gopalakrishnan, N. and Rao, A.R.M. (2014), "Low frequency and boundary condition effects on impedance based damage identification", *Case Studies in Nondestructive Testing and Evaluation*, **2**, 9-13.
- Rabelo D.S., Steffen, V., Neto, R.M.F. and Lacerda, H.B. (2017), "Impedance-based structural health monitoring and statistical method for threshold-level determination applied to 2024-T3 aluminum panels under varying temperature", *Struct. Health Monit.*, **16**(4), 1-17.
- Raju, V. (1998), "Implementing impedance-based health monitoring technique", Master Thesis, Virginia Polytechnic Institute and State University, Blacksburg, VA.
- Ritdumrongkul, S., Abe, M., Fujino, Y. and Miyashita, T. (2004), "Quantitative health monitoring of bolted joints using a piezoceramic actuator-sensor", *Smart Mater. Struct.*, **13**, 20-29.
- Ryu, J.Y., Huynh, T.C. and Kim, J.T. (2017), "Experimental investigation of magnetic-mount PZT-interface for impedance-based damage detection in steel girder connection", *Struct. Monit. Maint.*, **4**(3), 237-253
- Sepehry, N., Shamshirsaz, M. and Abdollahi, F. (2011), "Temperature variation effect compensation in impedance-based structural health monitoring using neural networks", *J. Intel. Mat. Syst. Str.*, **20**(10), 1-8.
- Siebel, T. and Lilov, M. (2013), "Experimental investigation on improving electromechanical impedance based damage detection by temperature compensation", *Key Eng. Mater.*, **569-570**, 1132-1139.
- Sodano, H.A., Park, G. and Inman, D.J. (2004), "An investigation into the performance of macro-fiber composites for sensing and structural vibration applications", *Mech. Syst. Signal Pr.*, **18**, 683-697.
- Soh, C.K., Tseng, K.K., Bhalla, S. and Gupta, A. (2000), "Performance of smart piezoceramic patches in health monitoring of a RC bridge", *Smart Mater. Struct.*, **9**, 533-542.
- Sohn, H. (2007) "Effects of environmental and operational variability on structural health monitoring", *Philos. T. R. Soc. A*, **365**, 539-560.
- Spencer, B.F., Ruiz-Sandoval, M.E. and Kurata, N. (2004), "Smart sensing technology: opportunities and challenges", *Struct. Control Health Monit.*, **11**, 349-368
- Stokes, J. P., and Cloud, G.L. (1993), "The application of interferometric techniques to the nondestructive inspection of fiber-reinforced materials", *Exper. Mech.*, **33**, 314-319.
- Studer, M. and Peters, K. (2004), "Multiscale sensing for damage identification", *Smart Mater. Struct.*, **13**(2), 283-294.
- Sun, F.P., Chaudhry Z., Liang, C. and Rogers C.A. (1995), "Truss structure integrity identification using PZT sensor-actuator", *J. Intel. Mat. Syst. Str.*, **6**, 134-139.
- Tibaduiza, D.A., Mujica, L.E. and Rodellar, J. (2013), "Damage classification in structural health monitoring using principle component analysis and self-organizing maps", *Struct. Control Health Monit.*, **20**, 1303-1316.

- Wang, D., Wang, Q., Wang, H. and Zhu H. (2016), "Experimental study on damage detection in timber specimens based on an electromechanical impedance technique and RMSD-based Mahalanobis distance", *Sensors*, 1-17.
- Woon, C.E. and Mitchell, L.D. (1996), "Variations in structural dynamic characteristics caused by changes in ambient temperature: Part I. Experimental", *Proceeding of the 14th IMAC, SEM*, 963-971.
- Yang, J., Zhu, H., Wang, D. and Ai, D. (2015), "The compensation technique of tensile force effect on the electro-mechanical impedance method for structural health monitoring", *J. Intel. Mat. Syst. Str.*, 1-12.
- Yang, Y. and Miao, A. (2010), "Two-dimensional modeling of the effects of external vibration on the PZT impedance signatures", *Smart Mater. Struct.*, **19**, 1-7.
- Yang, Y., Annamdas, V.G.M., Wang, C. and Zhou, Y. (2008), "Application of multiplexed FBG and PZT impedance sensors for health monitoring of rocks", *Sensors*, **8**, 271-289.
- Yun, C.; Cho, S.; Park, H.; Min, J. and Park, J. (2013), "Smart wireless sensing and assessment for civil infrastructure", *Struct. Infrastruct. Eng. Maint. Manag. Life-Cycle Design Perform.*, **10**(4), 534-550.
- Zagrai, A.N. and Giurgiutiu, V. (2001), "Electro-mechanical impedance method for crack detection in thin plates", *J. Intelligent Material Systems and Structures*, **12**, 709-718.
- Zahedi, F. and Huang, H. (2017), "Time–frequency analysis of electromechanical impedance (EMI) signature for physics-based damage detections using piezoelectric wafer active sensor (PWAS)", *Smart Mater. Struct.*, **26**, 1-9.

